Surname *et al. Microstruct* Year;Volume:Number
DOI: 10.20517/microstruct.xxx.xx

Microstructures

Open Access

Supplementary Material: An intriguing canting dipole configuration and its evolution under an electric field in La-doped Pb(Zr,Sn,Ti)O_3 perovskites

MAIN TEXT (optional)

3D electron diffraction data solution. The data were processed using the program REDp written by Wei Wan and Junliang Sun[1]. Using the program REDp, the diffraction peaks can be almost all indexed by the unit cell of a = 5.79221 Å, b = 5.79221 Å, c = 8.28519 Å, α = 90°, β = 90°, γ = 90°. It is worth noting that the 3D-ED is not completely kinematic, so the precise cell parameters and the atomic position need refinement by neutron diffraction.

Structure resolution using HR-NPD and HR-SXRD. The initial atomic positions were obtained by the Charge flipping algorithm[2] on Jana2006 software[3]. The precise crystallographic parameters were obtained by Rietveld refinement on Jana2006 software.

High-energy *in situ* synchrotron X-ray diffraction. *In situ* data were collected at 11-ID-C beamline at Advanced Photon Source, Argonne National Laboratory, USA, and the wavelength of X-ray is 0.1173 Å. The sample was a 5 mm × 1.2 mm × 0.6 mm bar cut from a ceramic disk. The schematic of experiment measurement can refer to our previous studies[4]. The precise crystallographic parameters were obtained by Rietveld refinement on GSAS-Ⅱ software[5].

Phase-field simulation. Phase-field simulation was performed to reveal the polarization switching in ferroelectric/antiferroelectric materials. Pb(Zr,Ti)O_3 single crystal was taken as an example by solving the time-dependent Ginzburg-Landau equation for the temporal evolution of the polarization vector field,

$$\frac{\partial P_i(\boldsymbol{r},t)}{\partial \mathrm{t}} = -L\frac{\delta F}{\delta \boldsymbol{P}_i(\boldsymbol{r},t)},\ (i=1,2,3)$$

where $\boldsymbol{P_i}(\boldsymbol{r},t)$ is polarization, L is the kinetic coefficient, and F is the total free energy of the system, which is expressed as,

$$\mathrm{F} = \iiint \left(f_{bulk} + f_{elas} + f_{elec} + f_{grad}\right)dV$$

where V is the system volume. The bulk energy density f_{bulk} can be calculated by,

$$\begin{aligned} f_{bulk} = {} & \alpha_1\left(P_1^2+P_2^2+P_3^2\right) + \alpha_{11}\left(P_1^4+P_2^4+P_3^4\right) + \alpha_{12}\left(P_1^2P_2^2+P_1^2P_3^2+P_2^2P_3^2\right) \\ & + \alpha_{112}\left[P_1^4\left(P_2^2+P_3^2\right)+P_2^4\left(P_1^2+P_3^2\right)+P_3^4\left(P_1^2+P_2^2\right)\right] \\ & + \alpha_{111}\left(P_1^6+P_2^6+P_3^6\right) + \alpha_{123}P_1^2P_2^2P_3^2 \end{aligned}$$

where P_1, P_2, P_3 are polarization components. α_1, α_{11}, α_{12}, α_{111}, α_{112} and α_{123} are Landau coefficients. The elastic energy density can be expressed as,

$$f_{elas} = C_{ijkl}\left(\varepsilon_{ij}-\varepsilon_{ij}^0\right)\left(\varepsilon_{kl}-\varepsilon_{kl}^0\right)$$

where C_{ijkl} is the elastic stiffness tensor, ε_{ij} and ε_{ij}^0 are the total local strain, and the spontaneous strain, respectively. The gradient energy density can be expressed as,

$$\begin{aligned} f_{grad} = {} & \frac{1}{2}G_{11}\left(P_{1,1}^2+P_{2,2}^2+P_{3,3}^2\right) + G_{12}\left(P_{1,1}P_{2,2}+P_{2,2}P_{3,3}+P_{1,1}P_{3,3}\right) \\ & + \frac{1}{2}G_{44}\left[(P_{1,2}+P_{2,1})^2+(P_{2,3}+P_{3,2})^2+(P_{1,3}+P_{3,1})^2\right] \\ & + \frac{1}{2}G'_{44}\left[(P_{1,2}-P_{2,1})^2+(P_{2,3}-P_{3,2})^2+(P_{1,3}-P_{3,1})^2\right] \\ & + g11\sum\nolimits_i\left(\frac{\partial^2 P_i}{\partial x_i^2}\right)^2 + g12\sum\nolimits_{i\neq j}\left(\frac{\partial^2 P_i}{\partial x_j^2}\right)^2 \end{aligned}$$

where G_{ij} is the gradient energy coefficients, f_{grad} is given in terms of the second-order derivative of the polarization[6], $g11$ and $g12$ are positive constants. The electric energy density f_{elec} is given by,

$$f_{elec} = -\frac{1}{2}\varepsilon_0\kappa_{ij}E_iE_j - E_iP_i$$

where E_i is the electric field component, which includes both the applied electric field and the depolarization field, ε_0 and κ_{ij} are the vaccum permittivity and dielectric constant, respectively.

The equation was solved by a semi-implicit Fourier spectral method[7] and the simulation size is 256 Δx × 256 Δx × 1Δx (Δx is the number of grid points and equals to 1 nm in this work) with the periodic boundary conditions in x, y, and z axes.

Supplementary Table 1. The orthorhombic cell parameters and *R* factors of

structure refinements using *Ima*2 as models

	HR-XRD	HR-NPD
Wavelength (Å)	0.4499	0.6225
a(Å)	5.77245(8)	
b(Å)	5.77524(8)	
c(Å)	8.14033(6)	
V(Å^3)	271.376(4)	
R_P(%)	5.35	7.29
R_{wp}(%)	5.71	7.64

HR-XRD: High-resolution X-ray diffraction; HR-NPD: high-resolution neutron powder diffraction.

Supplementary Table 2. The crystallographic parameters in Rietveld analysis of HR-SXRD and HR-NPD data for *Ima*2 PLZST were taken at room temperature (@ 0 kV/mm)

Atom	site	*x*	*y*	*z*	U_{iso}(Å^2)
Pb/La	4b	0.75	0.2497(8)	0.2903(16)	0.032(2)
Zr/Sn/Ti	4b	0.25	0.25374	0.04132	0.005(2)
O1	4a	0	0.5	0.0658(16)	0.023
O2	4a	0	0	0.0380(18)	0.023
O3	4b	0.25	0.1964(77)	0.2910(41)	0.023

HR-SXRD: High-resolution synchrotron X-ray diffraction; HR-NPD: high-resolution neutron powder diffraction; PLZST: $(Pb_{0.91}La_{0.06})(Zr_{0.42}Sn_{0.40}Ti_{0.18})O_3$.

Supplementary Table 3. The crystallographic parameters in Rietveld analysis for SXRD at 3 kV/mm

Atom	site	*x*	*y*	*z*	U_{iso}(Å^2)
Pb/La	4b	0.75	0.2494(8)	0.286(16)	0.031(2)
Zr/Sn/Ti	4b	0.25	0.247	0.035	0.005(2)
O1	4a	0	0.5	0.0649(16)	0.022

O2	4a	0	0	0.0383(18)	0.022
O3	4b	0.25	0.1964(17)	0.2913(1)	0.022
a = 5.7764(4) Å, b = 5.7729(4) Å, c = 8.1444(1) Å, R_{wp} = 3.55%					

SXRD: Synchrotron X-ray diffraction.

Supplementary Table 4. The crystallographic parameters in Rietveld analysis for SXRD at 6 kV/mm

Atom	**site**	***x***	***y***	***z***	$U_{iso}(Å^2)$
Pb/La	4b	0.75	0.2501(8)	0.283(2)	0.030(2)
Zr/Sn/Ti	4b	0.25	0.251	0.027	0.005(2)
O1	4a	0	0.5	0.0649(2)	0.023
O2	4a	0	0	0.0383(20)	0.023
O3	4b	0.25	0.196(5)	0.2913(41)	0.023
a = 5.7766(4) Å, b = 5.7716(3) Å, c = 8.1471(2) Å, R_{wp} = 3.6%					

SXRD: Synchrotron X-ray diffraction.

Supplementary Table 5. The Landau coefficients for the calculation of PZT[8]

Coefficient	**Formula**
α_1(C^{-2} m^2 N)	$(T-T_0)/(2\varepsilon_0 C_0)$
T_0 (℃)	$189.48 + 843.40x - 2105.5x^2 + 4041.8x^3 - 3828.3x^4 + 1337.8x^5$
η_1	$[2.6213 + 0.42743x + (9.6 + 0.012501x)e^{-12.6x}] \times 10^{14}/C_0$
η_2	$[0.887 + 0.76973x + (16.225 + 0.088651x)e^{-21.255x}] \times 10^{15}/C_0$
α_{11}(C^{-4} m^6 N)	$[10.612 - 22.655x + 10.955x^2] \times 10^{13}/C_0$
α_{12}(C^{-4} m^6 N)	$\eta_1/3.0-\alpha_{11}$
α_{111}(C^{-6} m^{10} N)	$[12.026 - 17.296x + 9.179x^2] \times 10^{13}/C_0$
α_{112}(C^{-6} m^{10} N)	$[4.2904 - 3.3754x + 58.804e^{-29.397x}] \times 10^{14}/C_0$

α_{123}(C^{-6} m^{10} N)	η_2-3.0×α_{111}-6.0×α_{112}
Q_{11}(C^{-2} m^2)	$\frac{0.029578}{1+200(x-0.5)^2}+0.042796x+0.045624$
Q_{12}(C^{-2} m^2)	$\frac{0.026568}{1+200(x-0.5)^2}+0.012093x+0.013386$
Q_{44}(C^{-2} m^2)	$0.5\times\left(\frac{0.025325}{1+200(x-0.5)^2}+0.020857x+0.046147\right)$

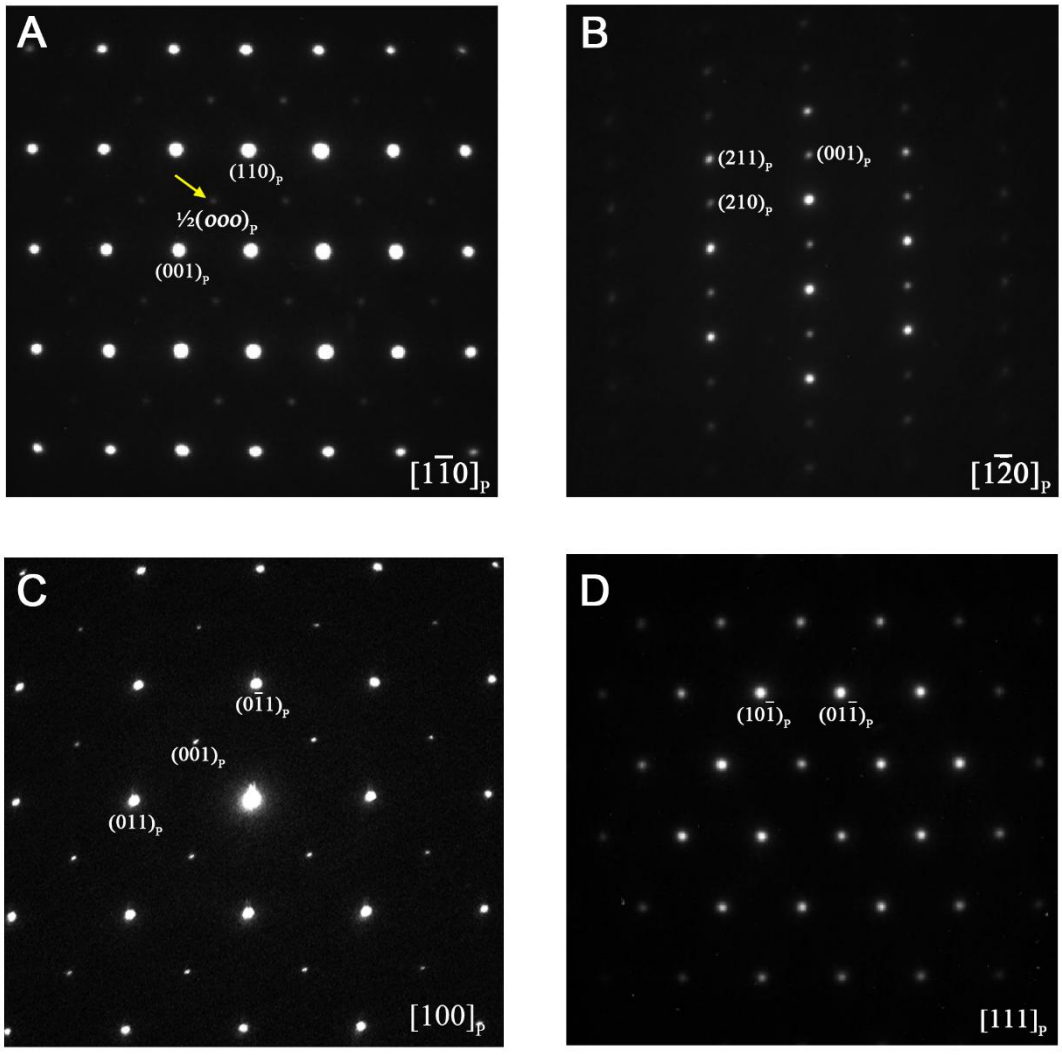

Supplementary Figure 1. The conventional TEM of PLZST. The diffraction reflection indicated by yellow arrows is produced by a commensurate structure, which is caused by the tilting of the oxygen octahedra. TEM: Transmission electron microscopy; PLZST: $(Pb_{0.91}La_{0.06})(Zr_{0.42}Sn_{0.40}Ti_{0.18})O_3$.

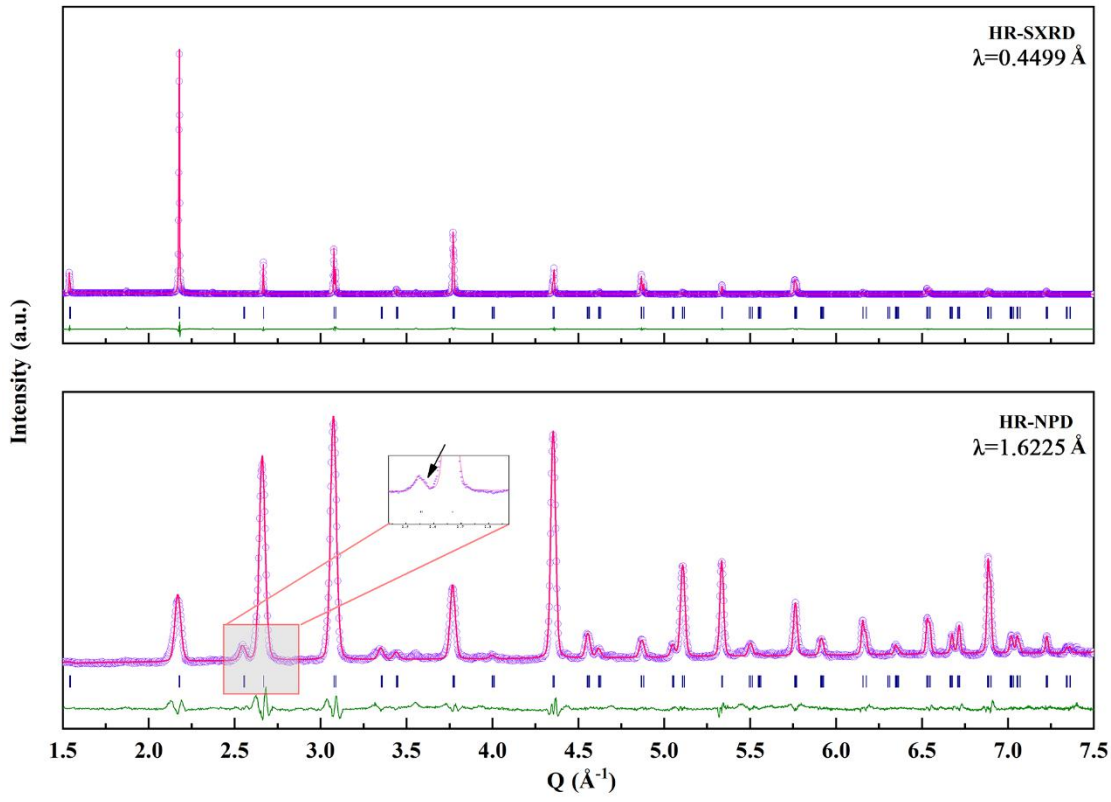

Supplementary Figure 2. Full-profile Rietveld refinement of orthorhombic phase of PLZST. Violet circle: observed data; Magenta line: calculate profile; Green line: the difference between the observed and calculated patterns; Blue bar: reflections of Bragg peak positions. The inset shows details of superlattice reflections (marked by a black arrow). HR-SXRD: High-resolution synchrotron X-ray diffraction; HR-NPD: high-resolution neutron powder diffraction.

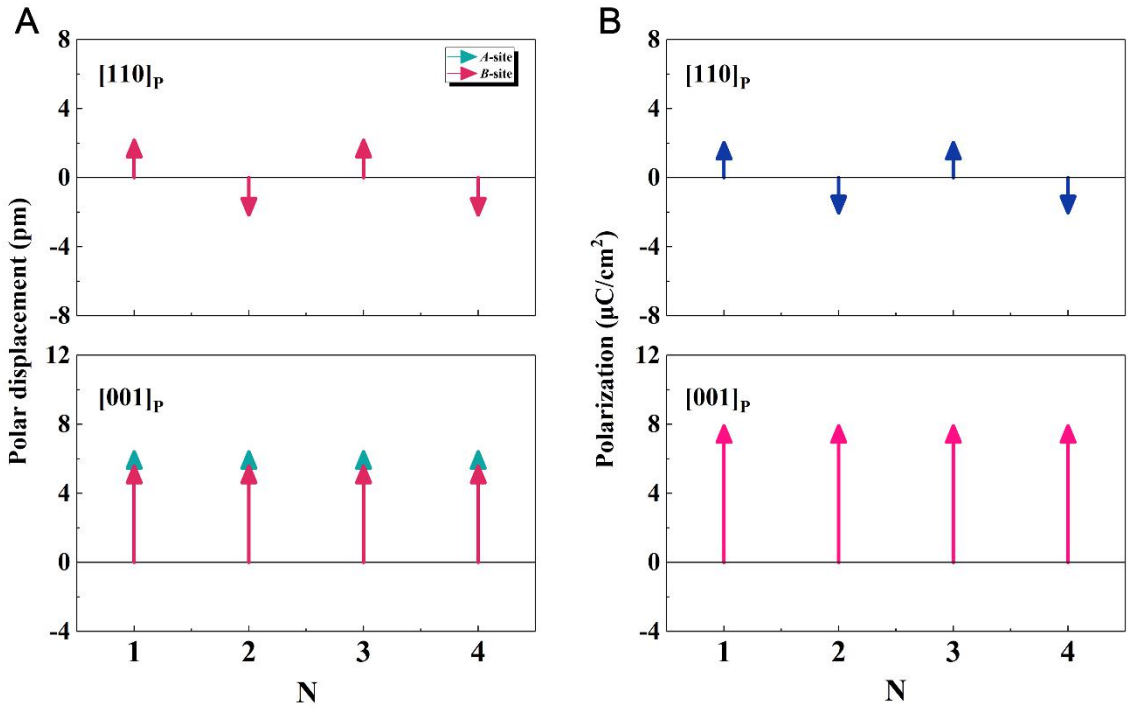

Supplementary Figure 3. (A) The polar displacement and (B) the polarization along the $[110]_P$ and the $[001]_P$ directions. The horizontal coordinate "N" represents the perovskite cell sequence. The polar displacement of *A*-site along the $[110]_P$ direction is zero in figure (a).

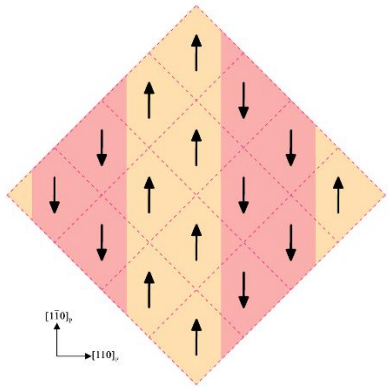

Supplementary Figure 4. The schematic of electric dipoles map of $PbZrO_3$[9].

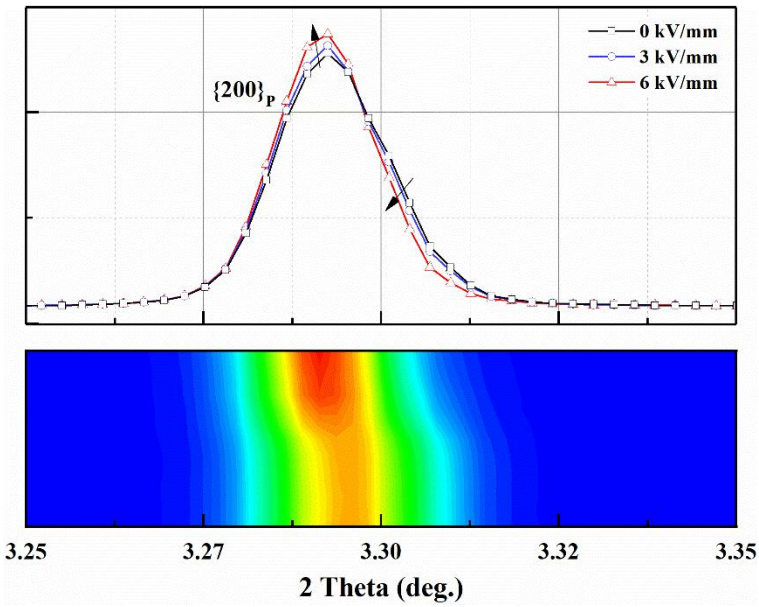

Supplementary Figure 5. Diffraction peak profiles and contour plots of $\{200\}_P$ as a function of the electric field at the 0° sector.

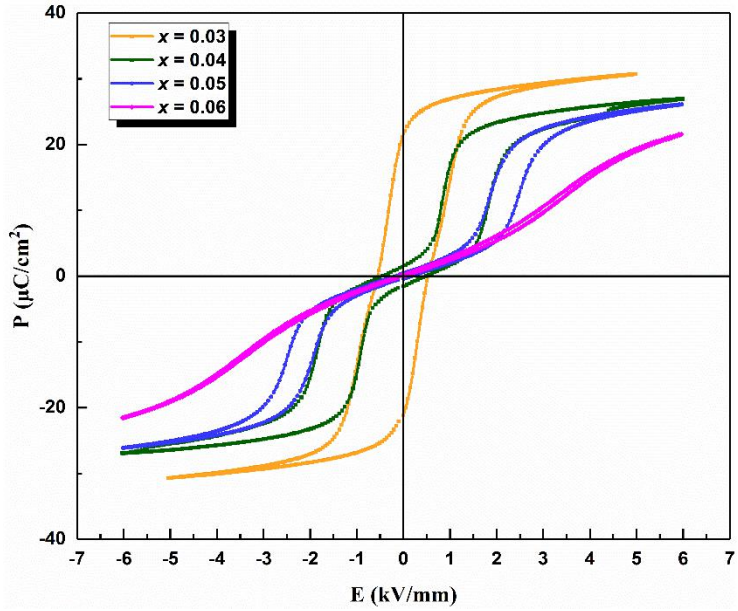

Supplementary Figure 6. The *P-E* loops of $Pb_{1-1.5x}La_xZr_{0.42}Sn_{0.40}Ti_{0.18}O_3$($x$ = 0.03, 0.04, 0.05 and 0.06).

REFERENCES

1. Zhang D, Oleynikov P, Hovmöller S, Zou X. Collecting 3D electron diffraction data by the rotation method. *Zeitschrift für Kristallographie* 2010;225:94-102.

2. Oszlányi G, Süto A. Ab initio structure solution by charge flipping. *Acta Crystallogr A* 2004;60:134-41.

3. Oszlányi G, Süto A. Ab initio structure solution by charge flipping. II. Use of weak reflections. *Acta Crystallogr A* 2005;61:147-52.

4. Petříček V, Dušek M, Palatinus L. Crystallographic computing system JANA2006: general features. *Zeitschrift für Kristallographie - Crystalline Materials* 2014;229:345-52.

5. Fan L, Chen J, Ren Y, Pan Z, Zhang L, Xing X. Unique piezoelectric properties of the monoclinic phase in $Pb(Zr,Ti)O_3$ ceramics: large lattice strain and negligible domain switching. *Phys Rev Lett* 2016;116:027601.

6. Liu Z, Xu B. Insight into perovskite antiferroelectric phases: landau theory and phase field study. *Scripta Materialia* 2020;186:136-41.

7. Chen L, Shen J. Applications of semi-implicit Fourier-spectral method to phase field equations. *Computer Physics Communications* 1998;108:147-58.

8. Haun MJ, Zhuang ZQ, Furman E, Jang SJ, Cross LE. Thermodynamic theory of the lead zirconate-titanate solid solution system, part III: curie constant and sixth-order polarization interaction dielectric stiffness coefficients. *Ferroelectrics* 1989;99:45-54.

9. Corker DL, Glazer AM, Dec J, Roleder K, Whatmore RW. A re-investigation of the crystal structure of the perovskite $PbZrO_3$ by X-ray and neutron diffraction. *Acta Crystallogr B Struct Sci* 1997;53:135-42.